JOURNAL OF AIRCRAFT
Vol. 46, No. 3, May–June 2009

Shock Effects on Delta Wing Vortex Breakdown

L. A. Schiavetta*
University of Glasgow, Glasgow, Scotland G12 8QQ, United Kingdom
O. J. Boelens†
National Aerospace Laboratory, NLR, 1006 BM Amsterdam, The Netherlands
S. Crippa‡
Royal Institute of Technology, 100 44 Stockholm, Sweden
R. M. Cummings§
U.S. Air Force Academy, USAFA Colorado 80840
W. Fritz¶
EADS Military Air Systems, 81633 Munich, Germany
and
K. J. Badcock**
University of Liverpool, Liverpool, England L69 7BZ, United Kingdom

DOI: 10.2514/1.38792

It has been observed that delta wings placed in a transonic freestream can experience a sudden movement of the vortex breakdown location as the angle of incidence is increased. The current paper uses computational fluid dynamics to examine this behavior in detail. The study shows that a shock/vortex interaction is responsible. The balance of the vortex strength and axial flow and the shock strength are examined to provide an explanation of the sensitivity of the breakdown location. Limited experimental data are available to supplement the computational fluid dynamics results in certain key respects, and the ideal synergy between computational fluid dynamics and experiments for this problem is considered.

Nomenclature

α	=	angle of attack
C_p	=	pressure coefficient
k	=	turbulent kinetic energy
M	=	Mach number
P_ω	=	Production of ω
p	=	pressure
Re	=	Reynolds Number
Ro	=	Rossby Number
s	=	wing span
U_θ, U_{axial}	=	tangential and axial velocity components
x	=	streamwise coordinate
x_{cr}	=	root chord
y	=	spanwise coordinate
ω	=	rate of dissipation of k

I. Introduction

THE occurrence of shocks on delta wings introduces complex shock/vortex interactions, particularly at moderate-to-high angles of incidence. These interactions can make a significant difference to the vortex breakdown behavior. For subsonic flows, the motion of the location of onset of breakdown toward the apex is relatively gradual with increasing incidence [1]. The strengthening of the shock that stands off the sting as the incidence is increased can lead to a shock/vortex interaction, triggering breakdown. The location of breakdown can shift upstream by as much as 30% of the chord in a single 1 deg incidence interval [2,3] due to this interaction.

From the study of the interaction between longitudinal vortices and normal shocks in supersonic flow [4], it has been found that it is possible for a vortex to pass through a normal shock without being weakened sufficiently to cause breakdown. The flow over slender delta wings is potentially more complex, as the shock is not necessarily normal to the freestream in the vortex core region [5]. Investigation is needed to consider the behavior and onset of vortex breakdown, particularly with respect to shock/vortex interactions.

To consider this behavior, the flow over a sharp-leading-edged slender delta wing was considered under subsonic and transonic conditions. This investigation was undertaken as part of the Second International Vortex Flow Experiment (VFE-2), a facet of the NATO Research and Technology Organization, Applied Vehicles Technology (RTO AVT-113) Task Group, which was set up to consider the flow behavior both experimentally and computationally over a specified 65 deg delta wing geometry. The work of VFE-2 built on the first International Vortex Flow Experiment (VFE-1) [6] carried out in the late 1980s, which was used to validate the inviscid computational fluid dynamics (CFD) codes of the time. Progress has been made in both experimental and computational aerodynamics, particularly in turbulence models, since the conclusion of the VFE-1. Therefore, it was proposed by Hummel and Redecker [7] that a second experiment should be undertaken to provide a new, comprehensive, database of results for various test conditions and flow regimes, to further the understanding of vortical flows. The test conditions considered under the VFE-2 framework include both subsonic and transonic Mach numbers for low, medium, and high angles of incidence at a range of Reynolds numbers [8].

The measured data at transonic conditions showed a sudden jump of the breakdown location toward the wing apex when a critical angle

Presented as Paper 0395 at the 46th AIAA Aerospace Sciences Meeting and Exhibit, Reno, NV, 7–10 January 2008; received 28 May 2008; revision received 24 February 2009; accepted for publication 24 February 2009.

*Ph.D. Candidate, Department of Aerospace Engineering.
†Research and Development Engineer, Applied Computational Fluid Dynamics, Department of Flight Physics and Loads, Aerospace Vehicles Division.
‡Research Scientist.
§Professor of Aeronautics, Department of Aeronautics. Associate Fellow AIAA.
¶Research and Development Engineer, Aerodynamics and Methods.
**Professor of Computational Aerodynamics, Department of Engineering. Member AIAA.

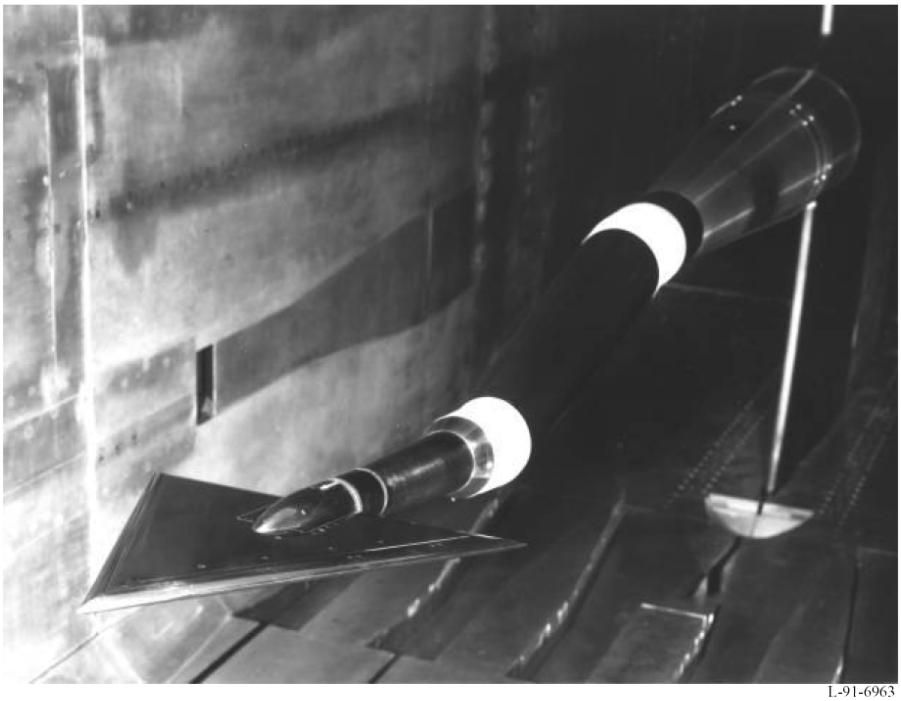

a) Wing in NTF facility at NASA Langley

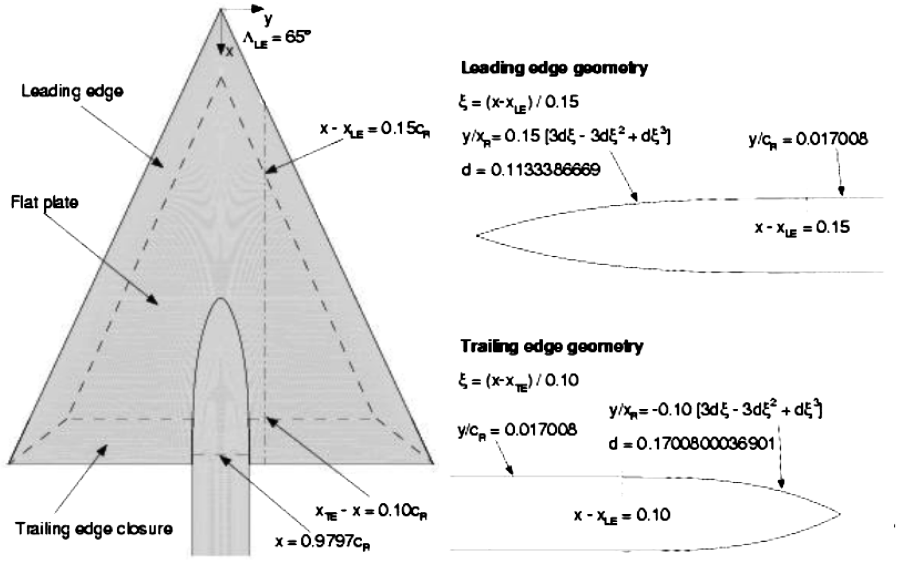

b) Definition of the wing geometry

Fig. 1 VFE-2 65 deg delta wing geometry used in the investigation. The photograph is reproduced from [9].

of incidence was reached. The current study uses CFD to investigate this effect toward an explanation of the detailed factors contributing to this behavior. The paper continues with a description of the test case and observed experimental behavior. A summary of a wide-ranging CFD study is then presented. Finally, the combined results are considered to produce an assessment of the mechanisms driving the flow behavior.

II. Experiments

The geometry used for the VFE-2 was originally tested in experiments carried out by Chu and Luckring [9–12] in the National Transonic Facility (NTF) at NASA Langley Research Center. These experiments considered a 65 deg delta wing with four leading-edge profiles (one sharp and three rounded with small, medium, and large radii) for a wide range of conditions, both subsonic and transonic, and for both test and flight Reynolds numbers. These data have been compiled into a comprehensive experimental database and formed the basis for the investigations of the VFE-2. The geometry is analytically defined for all leading-edge profiles. Both the medium-radius and sharp-leading-edge profiles are considered within VFE-2; however, for this investigation, only the sharp-leading-edge profile is considered. Figure 1 shows the wing situated in the NTF wind tunnel along with the information on the geometry.

The location of vortex breakdown for a freestream Mach number of 0.85 with incidence measured in the NTF [9] and in subsequent tests at DLR, German Aerospace Center [††] is plotted in Fig. 2. The CFD data also plotted in this figure are discussed later in this paper. The location of breakdown in the CFD results is extracted by finding where the axial flow goes to zero. For the experimental data, the exact location of vortex breakdown is not known; however, from the surface pressure coefficient distributions, the approximate locations

[††]Private communication with R. Konrath, 2007.

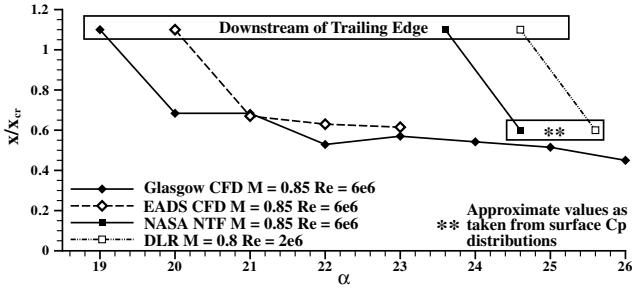

Fig. 2 Vortex breakdown locations for both computational and experimental results.

could be determined. The behavior of vortex breakdown is clear, with a sudden movement of the breakdown location toward the apex when a critical angle is reached. It is, however, difficult to see why this happens from the measured data. At least a larger density of pressure measurements is needed. In fact, it is seen from the CFD study that flowfield data are also needed to reveal details of the state of the vortex.

The objective of this paper is to use CFD to investigate the cause of the sudden motion of breakdown location toward the apex.

III. CFD Study

A CFD study was undertaken using several codes, grids, and modeling options. The purpose of this study was to see if the behavior observed in the measurements (i.e., the sudden jump in breakdown toward the apex) could be predicted and, if so, with what sensitivity to the details of the simulation. A summary of the codes and grids is given in Table 1.

A. Subsonic Results

First, a case at a freestream Mach number of 0.4 was computed. This case has no shock waves present. Two angles of incidence were calculated (at 18.5 deg, where no breakdown is present over the wing, and at 23 deg, where it is) and compared with the NTF measurements. Sample results are shown in Fig. 3, which compares the predictions of the University of Glasgow (Glasgow), National Aerospace Laboratory (NLR), and European Aeronautics and Defense Systems (EADS) simulations, with excellent agreement between all predictions and the measurements. This is typical of the expected performance of CFD codes for the prediction of pressures on a sharp-edged delta wing in subsonic flow, even if breakdown is present.

B. Transonic Results

Next, cases with a freestream Mach number of 0.85 were considered, where shock waves are expected to be present. The same angles of incidence were computed, with 18 deg again giving no breakdown over the wing and with 23 deg resulting in breakdown. The comparisons are shown in Fig. 4. The case before breakdown shows similar levels of agreement with the measurements. However, the case after breakdown shows significant discrepancies arising from the premature prediction of vortex breakdown. In fact, the sudden movement of breakdown is predicted about 3 deg earlier for the CFD when compared with the measurements. Note that in Fig. 4b, experimental results are included at 23.6 and 24.6 deg, and the large difference in pressure aft of $x/c = 0.5$ indicates that breakdown has moved rapidly up the wing between these two angles.

C. Location of Shock Waves in Glasgow Solution

Normal and crossflow shocks were found to occur in this flow. The main focus here is on the normal shocks, which can be identified by plotting the pressure coefficient along the symmetry plane, as shown in Fig. 5 for both angles of incidence. For the 18.5 deg case, it is clear that two normal shocks occur at the symmetry plane. The first occurs upstream of the sting tip at approximately $x/x_{cr} = 0.6$, and the second occurs downstream of the sting tip at approximately $x/x_{cr} = 0.85$, where a second shock is found. This second shock is likely to correspond to the rear/terminating shock, as described in the literature [2,5,17] for similar conditions. A third compression region is also found close to the trailing edge, and a third shock is found from the surface pressure contours at this location outboard of the symmetry plane on the wing surface. A shock occurring at this location is likely to be caused by the high curvature of the wing geometry and the necessity of the flow to return to freestream conditions at the trailing edge.

As the incidence is increased to 23 deg, vortex breakdown occurs on the wing, and the behavior at the symmetry plane again shows the shock in the vicinity of the sting tip at approximately $x/x_{cr} = 0.6$. However, another shock is also found in the flow slightly upstream of this location at about $x/x_{cr} = 0.52$. Downstream of the sting tip, it is evident that the rear/terminating shock described for the $\alpha = 18.5$ deg case is no longer present. Unsteady simulations at this angle showed that the flow is unsteady, with a complex shock motion cycle. This point is considered in detail in a subsequent section.

Considering the three-dimensional behavior of the normal shocks, it is found that the shock occurring upstream of the sting tip curves downstream and intersects the rolled-up shear layer of the vortex, as shown in Fig. 6 and highlighted by the dashed lines. This is also in agreement with the observations of Donohoe and Bannink [5]. Also highlighted are the locations of the other normal shocks described previously. The rear/terminating shock in the 18.5 deg solution is found to be normal to the freestream and wing surface and does not appear to curve downstream outboard of the symmetry plane. This lack of curvature may be due to the influence of the sting, as previous investigations have considered a flat wing without sting support [5].

D. Sensitivity Study

A sensitivity study was carried out to assess the CFD predictions of the sudden motion of the breakdown location. A large number of calculations [18–20] are summarized here. The conclusion in all cases is that the sudden motion of the breakdown location was present regardless of the details of the calculation used and that the critical angle is predicted to be lower in the computations than in the measurements.

1. Effect of Grid Refinement

The effect of grid refinement was considered for both pre- and postbreakdown flow for the transonic conditions using the Glasgow results. Comparisons of the surface pressure coefficient distributions

Table 1 Summary of grids and turbulence models used for VFE-2 structured grid comparisons. Coarse-grid dimensions are given in parentheses for the Glasgow code.

			No. of Grid Points on Wing			
Institution	Topology	Size × 10^6	Spanwise	Streamwise	Normal	Turbulence model[a]
EADS [13]	C-O	∼10.6	129	257	129	Wilcox k-ω and Reynolds stress model
NLR [14]	C-O	∼4	192	112	96	TNT k-ω with P_ω enhancer
Glasgow [15]	H-H with O-grid	∼7	170 (117)	228 (171)	81 (49)	Wilcox k-ω with P_ω enhancer and NLEVM
USAFA [16]	Unstructured	∼7.9	-	-	-	SA-DES $\Delta t = 0.0047$, 20,000 time steps
KTH	Unstructured	∼10.8	-	-	-	SA-DES $\Delta t = 0.0048$, 10,760 time steps

[a]NLEVM denotes nonlinear eddy viscosity method and SA-DES denotes Spalart–Allmaras detached eddy simulation.

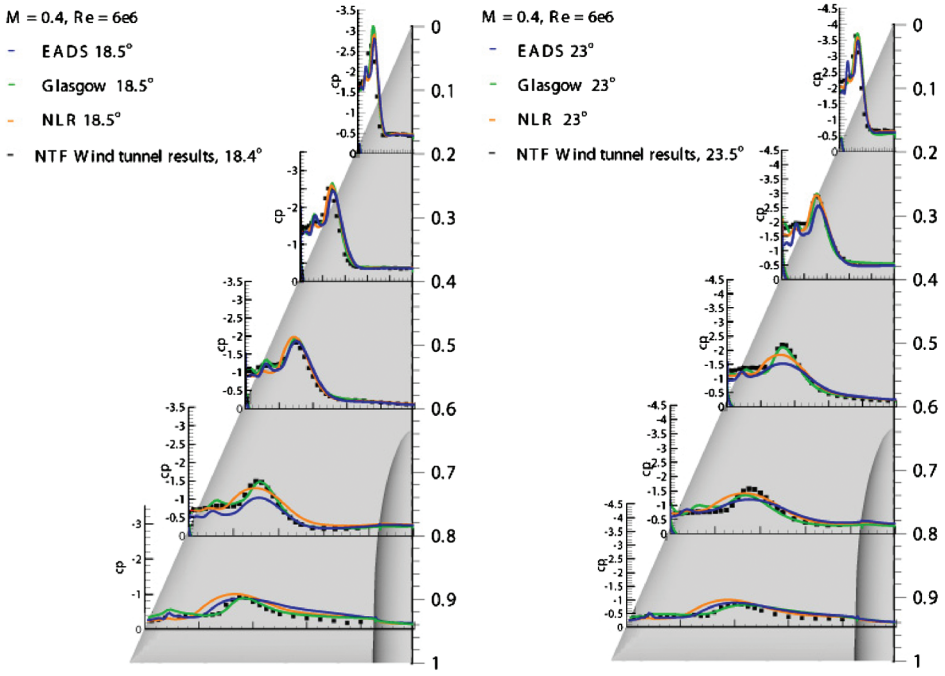

a) 18.5° b) 23°

Fig. 3 Comparison of computational results and experimental data at $M = 0.4$ and $Re = 6 \times 10^6$.

for both angles of incidence with the relevant experimental data are shown in Fig. 7. There are some differences in detail between the two solutions. However, the behavior and location of vortex breakdown are not greatly affected by the grid refinement carried out. It is also the case that the critical angle for vortex breakdown onset is independent of the grid refinement used, with vortex breakdown predicted to occur at lower angles of incidence on both grids.

2. *Effect of Turbulence Model*

The effect of the turbulence model on the flow behavior was considered by comparing results calculated using the k-ω with P_ω enhancer model and the nonlinear eddy viscosity model in the Glasgow code and the standard Wilcox k-ω and a Reynolds stress model (RSM) by EADS. The surface pressure coefficients are shown in Fig. 8. Each model predicts breakdown to occur on the wing at an incidence that is lower than that witnessed in the experiment. Some differences in the breakdown location are present due to the different vortex strengths predicted. However, the behavior of a rapid motion forward of the breakdown location is the same in each case.

3. *Comparison of Structured Grid Results*

Comparison of the structured solutions obtained at Glasgow, NLR, and EADS was made. The locations of the normal shocks in the flow solutions and the vortex breakdown locations are slightly

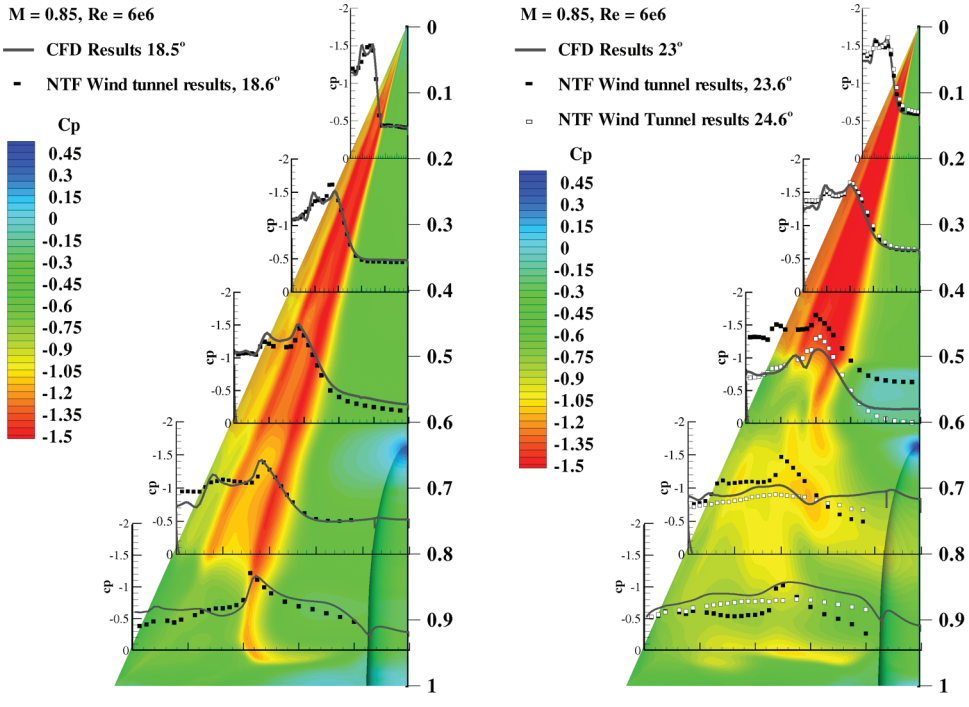

a) 18.5 deg b) 23 deg

Fig. 4 Comparison of computational results (Glasgow) and experimental data (NTF) at $M = 0.85$ and $Re = 6 \times 10^6$.

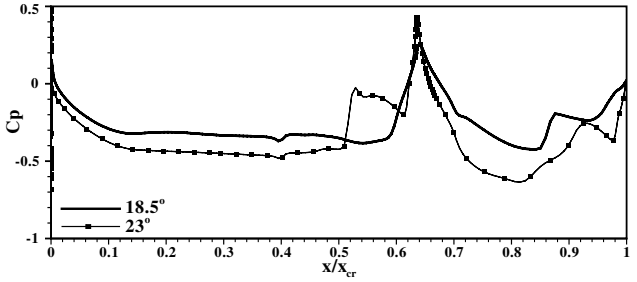

Fig. 5 Pressure coefficient distribution from Glasgow code at the symmetry plane on the wing for both angles of incidence.

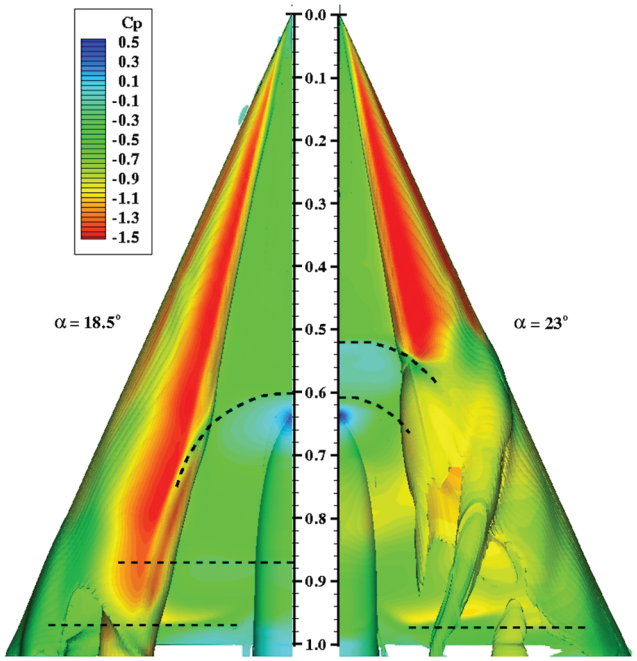

Fig. 6 Isosurface of x vorticity colored by pressure coefficient showing the primary vortex shear layer and normal shock shape for both angles of incidence (from the Glasgow code).

different for each solution, as shown in Fig. 9. These are likely to be due to the slightly different turbulence treatments and grids. However, the motion of the breakdown location is very similar in each case.

A comparison between the solutions for the Glasgow and NLR CFD solvers on a common grid was also performed. The turbulence models used by these two institutions are similar, with the difference mainly in the specification of the turbulence model diffusion coefficients [14]. The solutions obtained were very similar.

4. *Influence of Time Accuracy*

The comparison of surface pressure coefficient contours for the time-averaged U.S. Air Force Academy (USAFA) and Royal Institute of Technology (KTH) solutions shows an overall similar picture (see Fig. 10a). The USAFA solution shows a more pronounced shock upstream of the sting tip, which influences the interaction with the vortex. The KTH solution does not show such a distinct impact of the shock wave on the vortical system and presents a more diluted picture of the breakdown process. In general, there are some differences in breakdown location and shock strength; however, the behavior of the breakdown location motion is very similar in both cases. Analyzing the pressure coefficient fluctuations on the vortex core axis for the KTH solution reveals that the main region of influence of the fore-sting shock movement is between $x/c_r = 0.54$ and 0.72 (see Fig. 10b); hereafter, the fluctuations are due to the vortex breakdown unsteadiness. Time-accurate behavior of the shock and vortex breakdown movement is considered next.

IV. Evaluation

A. Shock-Vortex Interaction-Analysis Framework

From the CFD results, a shock ahead of the sting intersects the vortex system. It therefore seems possible that a shock/vortex interaction is important, particularly for higher angles of incidence. To consider this, the pressure in the freestream direction through the vortex cores for both angles of incidence was analyzed. This is shown in Fig. 11, with the calculated pressure ratios for each shock/vortex interaction location marked. For $\alpha = 18.5$ deg, the interactions occur without vortex breakdown. It has been previously suggested that this is due to the shock sitting above the vortex core [5].

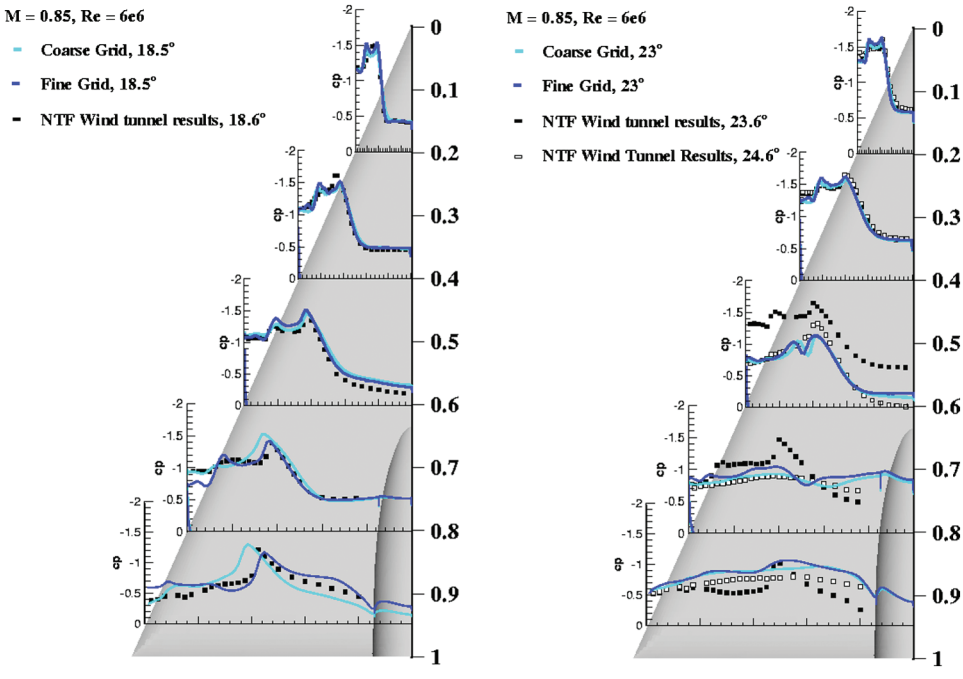

a) 18.5 deg **b) 23 deg**

Fig. 7 Comparison of Glasgow results between the H-H grids for transonic conditions at $\alpha = 18.5$ deg and 23 deg from the Glasgow code.

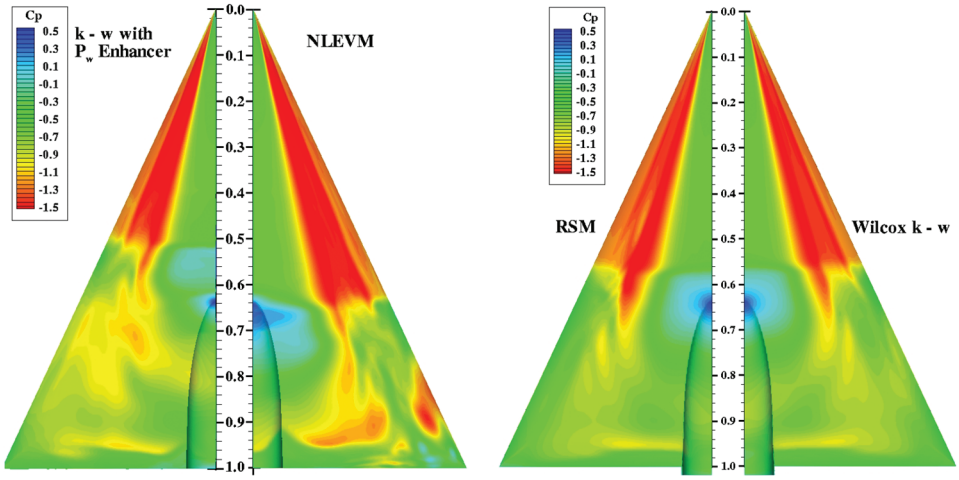

a) Comparison between NLEVM and k-ω with P_ω Enhancer model (Current Results)

b) Comparison between RSM and Wilcox k-ω model (EADS-MAS Results)

Fig. 8 Contours of surface pressure coefficient showing effect of turbulence model on flow solution for $\alpha = 23$ deg, $M = 0.85$, and $Re = 6 \times 10^6$.

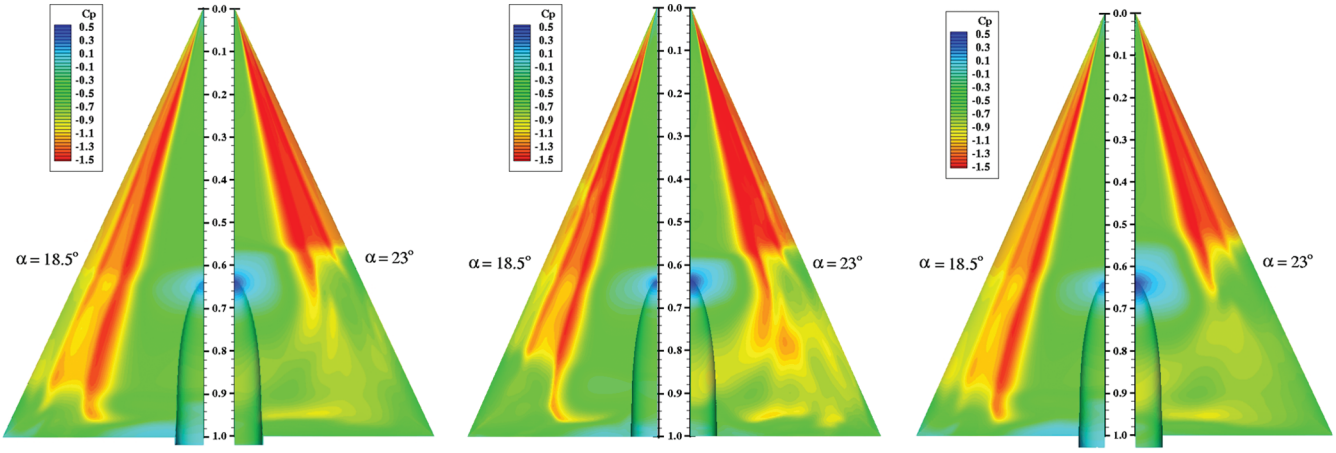

a) EADS-MAS b) Glasgow c) NLR

Fig. 9 Surface pressure coefficient contours for structured codes at $M = 0.85$ and $Re = 6 \times 10^6$.

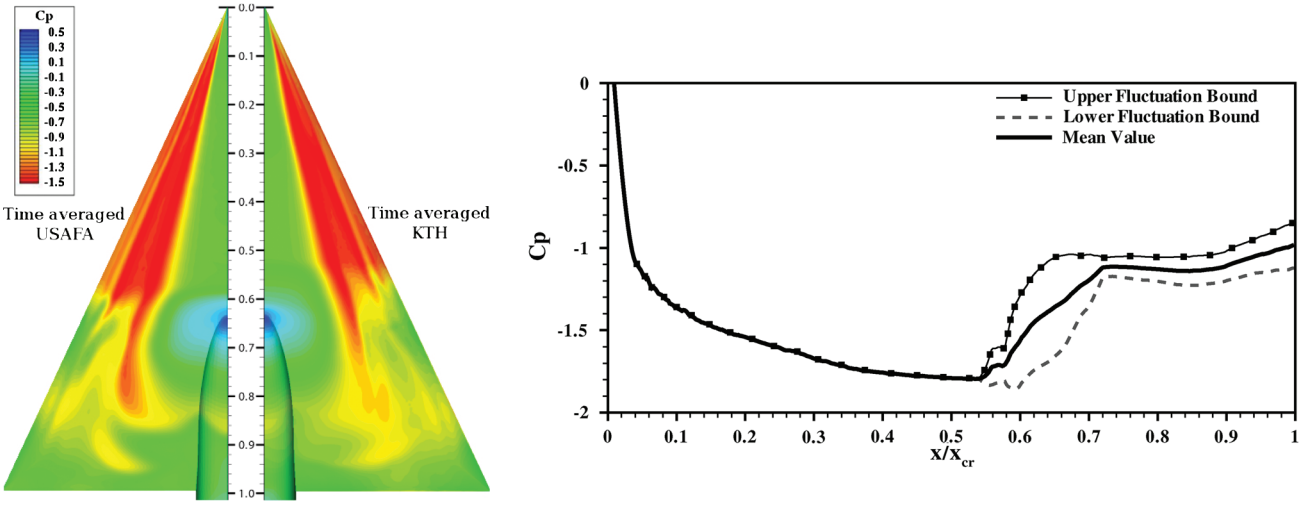

a) Comparison between USAFA and KTH results b) Pressure coefficient distribution through vortex core for KTH solution

Fig. 10 Time-averaged surface pressure coefficient contours for unsteady results at $M = 0.85$, $Re = 6 \times 10^6$, and $\alpha = 23$ deg.

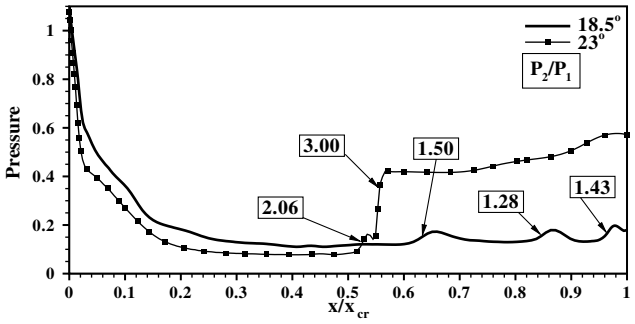

Fig. 11 Pressure distribution (from the Glasgow code) through vortex cores for both angles of incidence. The numbers on the plot signify the magnitudes of the pressure ratios through the intersecting shocks.

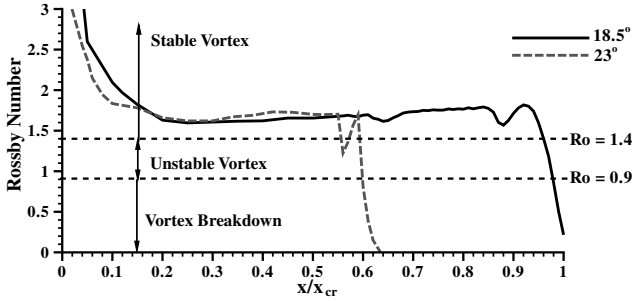

Fig. 12 Rossby number distribution from the KTH code against root chord location for pre- and postbreakdown cases.

However, from consideration of the vortex core properties, it is found that there are three regions of adverse pressure gradient that will influence the vortex. These coincide with the two normal shocks at the symmetry plane and the trailing-edge shock, as described previously, and are clear from Fig. 6. The pressure ratios for all three regions are less than 1.5 and, as shown, the primary vortex recovers after passing through each. Therefore, it may be suggested that these are weak interactions.

At $\alpha = 23$ deg, where breakdown occurs on the wing, it is clear that there are two regions of high adverse pressure gradient at the vortex core. The first coincides with the location of the normal shock upstream of the sting tip, as shown at the symmetry plane in Fig. 5. Very close to this, the second, higher, pressure gradient coincides with the occurrence of vortex breakdown. These pressure gradients have ratios of 2.00 and 2.36, respectively. It is likely that the first pressure increase is due to the effect of the normal shock at the symmetry plane on the vortex core, in a similar manner to the interaction at the lower incidence.

There are interactions between the shocks and vortex core for both angles of incidence, with a weaker interaction occurring for the lower incidence. It is suggested that there is a limiting behavior below which the vortex can feel the effects of the shock and remain coherent. Above this limit, the interaction causes a considerable weakening of the vortex core, which results in vortex breakdown. In his comprehensive review, Deléry [21] demonstrated the importance of a number of parameters for vortex breakdown caused by shock/vortex interaction. These include the tangential or swirl velocity U_θ and the axial velocity of the vortex core, U_{axial}. He also proposed that the swirl ratio or the Rossby number may be used as a measure of the vortex intensity and thus of the susceptibility of the vortex to shock-induced breakdown. The Rossby number is a nondimensional parameter, defined as the ratio of the axial and circumferential momentum in a vortex, as defined by Eq. (1). In this investigation, the maximum axial velocity at the vortex core and the maximum swirl velocity of the vortex are used. This relationship is the inverse of the axial swirl parameter [21], which is used as a breakdown criterion for a free vortex:

$$Ro = \frac{U_{\text{axial}}}{U_\theta} \tag{1}$$

As a vortex passes through a normal shock, the tangential velocity is found to stay relatively constant, whereas the axial velocity decreases, therefore reducing the Rossby number [22]. With the reduction in the Rossby number comes an increase in vortex intensity and, as a result, the susceptibility of the vortex to breakdown increases. A criterion for breakdown using the Rossby number has also been investigated by Spall et al. [23] and by Robinson et al. [24], who applied it to computational results on slender delta wings and determined that the limiting Rossby number occurs between 0.9 and 1.4 for most cases, with a stable vortex core occurring for values above 1.4. To consider this criterion, the Rossby number was calculated for both pre- and postbreakdown angles of incidence, and the resulting graph is shown in Fig. 12 with respect to streamwise location on the wing. Also noted on the plot are the critical Rossby numbers for vortex breakdown.

These results also show the influence of the shocks on the vortex behavior. At $\alpha = 18.5$ deg, it is clear that weak interactions occur as the Rossby number decreases. However, this reduction is not significant, which shows that the vortex is not sufficiently weakened by the shock. A recovery is witnessed downstream. At $\alpha = 23$ deg, a similar behavior is noted at $x/c_r = 0.58$, where the vortex is affected by the normal shock. However, the reduction in Rossby number is greater than for $\alpha = 18.5$ deg, and the vortex becomes unstable. Vortex breakdown is then caused by a second shock at approximately $x/c_r = 0.62$, which has a greater effect on the already weakened vortex axial flow, and breakdown is almost immediate.

B. Quantitative Assessment

The strength of the impinging shocks should be considered pre- and postbreakdown. Unfortunately, little experimental data exist to allow the shock strength to be measured through the vortex core. However, the strength of the shocks incident on the surface of the wing may be considered to improve confidence in the computational solutions. Unfortunately, there are only five data points from the NTF data; however, the presence of an increase in pressure between $x/c_r = 0.6$ and 0.8 for the 23.6 deg incidence and $x/c_r = 0.4$ and 0.6 for the 24.6 deg incidence is still clear. As the sting tip is located at approximately $x/c_r = 0.64$, these pressure jumps are most likely to be located close to the $x/c_r = 0.6$ streamwise location. Using this as a guide, an approximation to the shock strength at this location can be determined. The approximate values calculated are given in Table 2.

Using the values in Table 2 as a guide, it is evident that there is a considerable difference in the calculated pressure changes at the sting tip location for the pre- and postbreakdown experimental results. The calculated pressure ratio for the postbreakdown case is roughly 25% larger than for the prebreakdown case. Similar distributions were also obtained from the computational solutions for the pre- and postbreakdown cases, and the shock strengths calculated are also stated in Table 2. From a comparison with the experimental data, it is clear that the magnitude of the postbreakdown pressure ratio is very similar; however, the prebreakdown ratio is larger. This means that, overall, the increase between the pre- and postbreakdown cases for the computational results is less. The larger pressure ratio of the computational results for the prebreakdown case may have implications for the onset of breakdown. If the shock strength is overpredicted in the computational results, it is likely that breakdown would occur closer to the apex, compared with the experimental results for a given vortex strength.

Table 2 Summary of shock strength from the Glasgow code on surface conical ray at constant $y/s = 0.3$ for all solutions at $M = 0.85$ and $Re = 6 \times 10^6$ compared with NASA NTF data

Source of data	P_2/P_1
NASA NTF experiment: 23.6 deg	1.16
NASA NTF experiment: 24.6 deg	1.4673
CFD-18.5 deg	1.2314
CFD-23 deg	1.4695

Table 3 Summary of shock and vortex core data for all steady-state calculations using the Glasgow code at $\alpha = 18.5$–26 deg, $M = 0.85$, and $Re = 6 \times 10^6$

α	VBD?	Maximum U_{axial}[a]	Maximum M_{axial}	P_2/P_1	Shock x/c_r
18.5 deg	No	1.74	1.76	1.5	0.62
19 deg	No	1.76	1.80	1.67	0.64
20 deg	Yes	1.74	1.83	3.73	0.64
21 deg	Yes	1.74	1.86	4.87	0.64
22 deg	Yes	1.79	1.88	4.67	0.51
23 deg	Yes	1.80	1.92	5.25	0.55
24 deg	Yes	1.84	2.05	5.93	0.49
25 deg	Yes	1.84	2.10	5.64	0.47
26 deg	Yes	1.84	2.20	5.48	0.40

[a]The reference velocity for U_{axial} is taken to be the freestream speed.

Table 4 Summary of maximum axial velocity, shock strength. and breakdown location for all solutions at $\alpha = 23$ deg, $M = 0.85$, and $Re = 6 \times 10^6$

				Vortex core shocks			Shock at $y/s = 0.3$:	
CFD solution	U_{axial}	M_{axial}	Ro	First P_2/P_1	Second P_2/P_1	Total P_2/P_1	P_2/P_1	VBD x/c_r
EADS	1.50	——	~1.67	1.77	1.64	2.55	1.4274	0.68
Glasgow	1.83	2.00	~1.7	2.00	2.36	4.75	1.4695	0.64
NLR	1.60	——	~1.74	1.50	2.89	4.33	1.5075	0.67
USAFA (time-averaged)	1.80	2.03	~1.67	——	——	4.50	1.4409	0.68
USAFA (instantaneous)	——	——	——	2.51	2.71	4.75	——	0.66
KTH (time-averaged)	1.79	1.87	~1.72	——	——	4.72	1.468	0.67

To consider the incidence at which vortex breakdown first occurs on the wing and the relative strength of the shocks, additional calculations were performed for intermediate angles of incidence between 18.5 and 26 deg for the same flow conditions as before ($M = 0.85$ and $Re = 6 \times 10^6$). A summary of the important flow details is shown in Table 3. These details include whether vortex breakdown occurred, the maximum vortex core axial velocity, Mach number, and the strengths and locations of the first impinging shock at each incidence. From the analysis, it was found that the 23 deg case was the only incidence to exhibit the double shock at vortex breakdown, and so the combined shock strength is instead shown for comparison with the other results. More is said subsequently about the shock pattern.

Before considering the onset of breakdown, it is important to note the behavior of the flow variables with increasing incidence. It is clear from Table 3 that the predicted shock strength increases with incidence, which is in agreement with the experimental data in Table 2. The axial velocity and Mach number are also found to increase; however, the Rossby number was found to be constant at ≈ 1.7 for each incidence, as described before. From the theory of supersonic flows, it is known that the strength of a shock is dependent on the upstream Mach number; thus, for a higher axial flow, a stronger shock will occur. However, in this case, the relationship does not appear to be linear. This is most likely to be due to changes in the shape of the shock in response to changes in the flow behavior and the equilibrium conditions as the incidence is increased. This may also suggest that the behavior of the vortex breakdown is also nonlinear with incidence.

Vortex breakdown first appears on the wing at $\alpha = 20$ deg, which coincides with a significant increase in shock strength. At this point, it may be assumed that the strength of the shock is high enough to cause a complete reorganization of the flow behavior. Thus, the shock strength limit for breakdown for these solutions may be given as 3.73. To determine a link between the vortex flow conditions, as described by the Rossby number, and the shock strength for breakdown to occur on the wing, further data, both experimental and computational, is needed.

To further consider the relation between the occurrence of breakdown, the vortex core behavior, and the predicted shock strength, the vortex core data for the EADS-MAS (Military Air Systems), NLR, and time-averaged USAFA results are considered in a similar manner. The pressure behavior through the vortex core, with the pressure ratios marked, is shown in Fig. 13. From this plot, it is clear that a similar behavior occurs, with shocks intersecting the vortex core axis and vortex breakdown occurring. From the EADS-MAS and NLR solutions, the pressure ratios through the shocks are approximately 1.77 and 1.64, and 1.5 and 2.89, respectively. The USAFA time-averaged solution has only one shock region, with a ratio of 4.5. However, from analysis of the instantaneous solutions, it was found that two shocks also exist at breakdown, which for the solution at a time step of $\tau = 16,600$ correspond to 2.25 and 2.71.

Although the predicted strength of a shock can be dependent on such factors as grid refinement, turbulence model, and discretization, it is also apparent that there are corresponding differences in predicted maximum axial velocity through the vortex core, as summarized in Table 4. The Glasgow solution has predicted a maximum axial velocity that is the same as the USAFA solutions and higher than for the EADS-MAS and NLR solutions. As a result of this increase in axial velocity, the Mach number upstream of the shock will increase, and the upstream pressure will reduce, resulting in a stronger shock to maintain equilibrium. However, it is evident that the Rossby number in each case is similar. This suggests that the shock strength predicted by the computational solutions is dependent on the vortex core behavior predicted upstream. The axial flow behavior is also dependent on the computational parameters mentioned previously. However, despite the differences in flow solutions and computational setup, the behavior and effect of the shocks on the flow are the same.

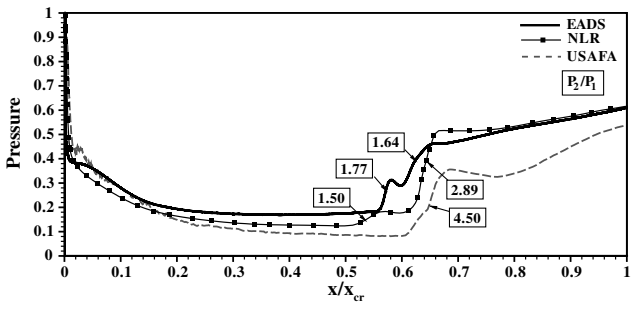

Fig. 13 Pressure distribution through vortex cores for EADS, NLR and USAFA (time-averaged) solutions.

C. Validation of the Axial Flow Predictions

To consider the ability of the computational solutions to predict the axial flow upstream of breakdown, the particle image velocimetry (PIV) results obtained at DLR (see footnote [††]) were considered. These experiments were carried out for slightly different flow conditions, with a Mach number of $M = 0.80$ and Reynolds number of $Re = 3 \times 10^6$. To compare with these results, a new set of calculations was performed by Glasgow, using the k-ω with P_ω enhancer turbulence model for $M = 0.80$ and $Re = 2 \times 10^6$ at angles of incidence of $\alpha = 18.5$–26 deg. Figure 14 shows a comparison of the crossflow behavior for a nominal incidence of $\alpha = 26$ deg. The effect of the difference in Reynolds numbers should be negligible, due to the sharp leading edge. In the experiment, it was found that vortex breakdown occurred between the $x/c_r = 0.6$ and 0.7 streamwise stations. However, the computations predict breakdown further upstream at $x/c_r = 0.4$. Therefore, to make a comparison of the prebreakdown flow, the results were compared on planes that were a similar nondimensional distance from the breakdown location; this corresponds to $x/c_r = 0.5$ for the experiment and $x/c_r = 0.3$ for the computational results, assuming that the breakdown occurs close to the $x/c_r = 0.6$ location. From the comparisons of the nondimensional u velocity contours, a number of observations may be made. It is clear that the location of the vortex core is very different between the computational and experimental results; however, this is likely to be due to the proximity of the computational slice to the apex of the wing, as further downstream the vortex would lift further from the wing surface. However, the shape of the vortical system is the same, with a very elongated primary vortex in both sets of results. Considering the vortex core properties from the experimental data at three prebreakdown PIV planes, it was found that the u velocity corresponds to 1.962 at $x/c_r = 0.5$, 1.870 at $x/c_r = 0.55$, and 1.522 at $x/c_r = 0.6$. Although the maximum velocity found from the measurement planes is 1.962, it is likely that the actual maximum velocity will be larger. The maximum u velocity for the computational results corresponds to $u = 1.88$, which is slightly lower than the maximum experimental value. Therefore, it is possible that the axial flow behavior is underpredicted in the computational solutions.

D. Shock Behavior in Unsteady Solutions

The analysis of all contributed RANS and the time-averaged detached eddy simulation (DES) computations reveals the presence of either one or two shocks upstream of the sting–wing intersection. To understand this discrepancy between the otherwise similar solutions, it is necessary to assess the time-dependent flowfield. In this section, the DES computations performed at KTH have been evaluated. This analysis enables helps to explain the postbreakdown development of the main vortical structures and also the complex interaction between vortex breakdown and the shock system ahead of the sting.

Figure 15 shows the vortex breakdown position history for the last cycle of the KTH solution. The position of breakdown is defined here as the foremost chordwise station in which there is fully reversed axial flow in the primary vortex. Details of the time steps indicated in Fig. 16 are shown in Fig. 15.

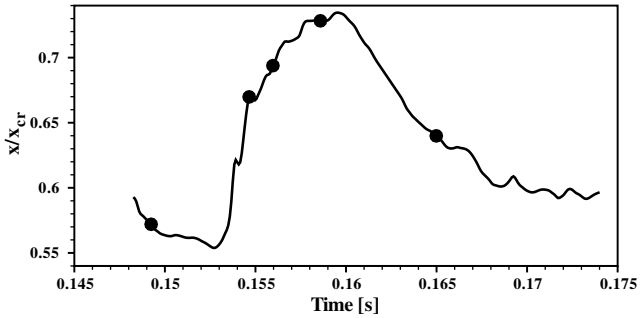

Fig. 15 Vortex breakdown position for the KTH solution; time steps presented in Fig. 16 are highlighted.

It is apparent from Fig. 15 that the downstream movement occurs relatively suddenly and the upstream recovery is more gradual. The USAFA DES predictions show a similar behavior. Because the flowfield features several minor complex shock systems in the postbreakdown region, it is useful to constrain the analysis to a single plane. The reason for the different behavior of the downstream and upstream motion can be found from the flowfield at the symmetry plane.

At the earliest time, a single shock wave is found to propagate upstream ahead of the sting tip at $x/c_r \approx 0.51$. A further supersonic region is present above the sting, aft of the sting tip (see Fig. 16a). In a subsequent time step, the second shock region forms a supersonic bridge to the flat-plate wing portion, right ahead of the sting tip, effectively resulting in a twin-shock fore-sting system. The first, now weaker, shock moved slightly more upstream than the aforementioned position at $x/c_r \approx 0.48$ and a second shock was placed right in front of the sting–wing intersection at $x/c_r \approx 0.6$ (see Fig. 16b). Because of this peculiar arrangement, the vortex breakdown position moves abruptly from downstream of the (first) shock impinging on the vortex core, visible in Fig. 16a downstream of the second shock, as visible in Fig. 16b. The relaying mechanism from the first to the second shock is what causes the abrupt downstream movement of the vortex breakdown position. When the two supersonic regions merge (Fig. 16c), the downstream motion of the strong single shock still continues slowly toward the sting tip. A further downstream motion of the shock is halted by the presence of the sting tip. The furthermost downstream position of the vortex breakdown is reached at $x/c_r \approx 0.61$, when the bent-field shock surface is weak enough to relieve the primary vortex core from the sudden pressure jump (see Fig. 16d). Now the vortex breakdown location starts to move upstream, following a discernible lag in the upstream movement of the shock wave. In contrast to the

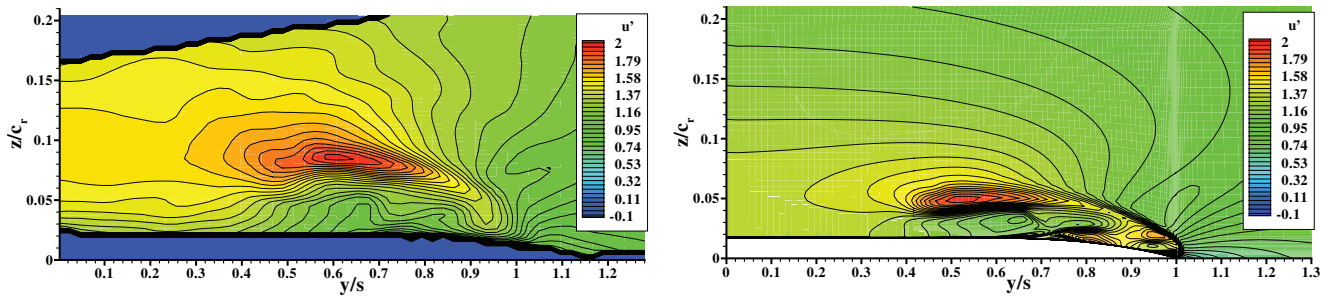

a) PIV, $\alpha = 25.9°$, $Re = 3 \times 10^6$ **b) CFD, $\alpha = 26°$, $Re = 2 \times 10^6$**

Fig. 14 Comparison between u velocity contours for experimental PIV and computational results for $M = 0.80$ on a slice at $x/c_r = 0.5$.

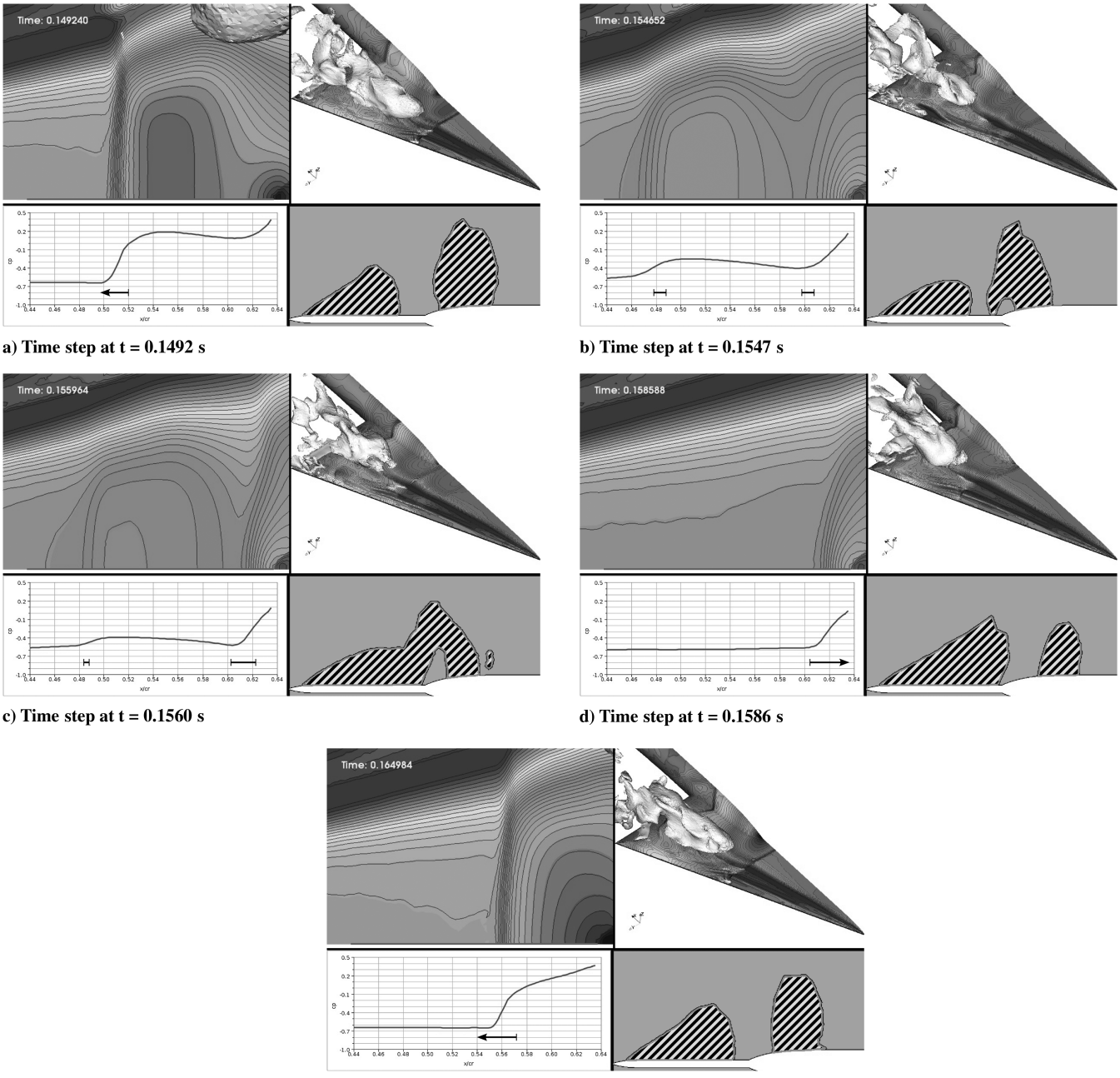

a) Time step at t = 0.1492 s

b) Time step at t = 0.1547 s

c) Time step at t = 0.1560 s

d) Time step at t = 0.1586 s

e) Time step at t = 0.1650 s

Fig. 16 Subframes presented in clockwise order, starting from the lower-right corner: symmetry plane showing the Mach number; frontal isometric view of the half-span suction side showing surface c_p and the reversed flow isosurface; wall-normal view on the suction side in front of the sting–wing intersection showing surface c_p; and c_p at the intersection of the symmetry plane and wing surface, $x/c_r = 0.44$–0.635.

downstream movement, during the upstream movement, the shock does not split in two. A gradual decrease in the strength of the single fore-sting shock is detectable, and the size of the supersonic region on the sting simultaneously increases (see Fig. 16e). The next cycle starts only then, when the single fore-sting shock reaches its furthermost upstream position, which is coupled to a decrease of the shock strength. From the time-dependent solution, it is possible to recognize disturbances in the region between the single fore-sting shock, the sting tip, and the primary vortex. These disturbances propagate upstream from the sting tip and move toward the single shock. The frequencies of the upstream moving disturbances and the spiral motion of the disrupted vortex core are very similar. These disturbances, originating from the postbreakdown vortex filaments, could be the initial triggering mechanism behind the split of the single shock wave into two weaker ones.

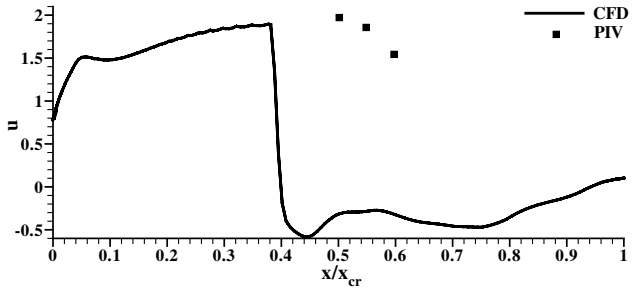

Fig. 17 Velocity of u through the vortex core for computational results compared with experimental PIV data for $M = 0.80$ and $\alpha = 26$ deg.

E. Motion of Vortex Breakdown Location

Having considered the mechanisms that cause vortex breakdown to occur on the wing, it is possible to return to the issue of the discrepancies between the CFD and experimental results. It was found from the experimental data used in this study that vortex breakdown jumps abruptly from a location downstream of the trailing edge to a location upstream on the wing for a small increase in incidence. Indeed, from the results summarized in Table 3, it is clear that the flow seems to go from full vortical flow over the whole wing surface to breakdown occurring close to the $x/c_r = 0.6$ location in a 1 deg increase.

From the plot in Fig. 2, it is clear that the behavior at the onset of vortex breakdown is qualitatively similar for both the CFD and experiment; however, the angle at which this occurs varies. With further consideration of the literature, it was found that there is a large spread of values for this critical angle. These are detailed in Table 5. It is quite clear from all these results that the critical onset angles for vortex breakdown over the wings for current CFD solutions are consistently earlier than for the majority of the experimental results. As shown, with an increase in incidence, the strength of the shocks in the flow increases, most likely as a response to the increased flow acceleration over the wing surface. Similarly, the axial velocity in the vortex core increases, and it has been shown that there is a critical relationship between these quantities that results in breakdown for a critical incidence. To change the angle at which vortex breakdown occurs, it will be necessary to have a change in either one of these parameters. For example, with an increase in vortex intensity and therefore a decrease in axial velocity or an increase in tangential velocity, the strength of the shock needed to cause breakdown will decrease and breakdown will occur earlier on the wing.

From the results detailed in the previous section, it is suggested that two factors are causing the early prediction of breakdown on the wing. These are an underprediction of the axial velocity, which results in a vortex more susceptible to breakdown, and an overprediction of the strength of the shocks. From consideration of the effects of a number of flow parameters, it appears that these predictions are not greatly effected by grid structure, turbulence model, convergence, or time accuracy. The effect of grid refinement was also considered, which also concluded that the overall refinement of the grid had little effect on the solution. However, this study did not consider localized refinement, particularly in the vortex core region. Despite continuing improvement in CFD codes, turbulence models, and practices, prediction of the vortex core behavior and axial flow is still a challenge. There have been a number of collaborations and investigations that have considered the vortical flows over delta wings, which have also generally predicted the flow behavior well; however, the axial velocity is almost always much lower than that found from experiments. This is also true for this case and may be attributed to the abilities of turbulence modeling and restrictions in grid refinement for the core region. To fully resolve the vortex core behavior, it would be necessary to have similar refinement to that applied to boundary-layer regions. It is unclear at this time whether an improvement in vortex core axial velocity would alter the predicted strength of the shocks in the flow; however, if the shock strength remained constant, with an increase in axial velocity, it may be suggested that the angle of incidence at which breakdown occurred would increase.

V. Conclusions

A CFD study, which employed several different codes and formulations, was used to investigate the possible causes of the sudden motion of vortex breakdown toward the apex with increasing angle of attack for the transonic flow over a 65 deg sharp edge delta wing. This behavior had previously been observed in measurements, but insufficient detail was available to understand the causes. The CFD predictions showed qualitatively similar behavior to the measurements, but the rapid motion of breakdown happened at a different angle of attack.

The CFD results showed a remarkable degree of consistency despite a range of turbulence treatments, grids, and time accuracy or steady-state solutions being used. In all cases, the critical angle was predicted 3 deg earlier than in the measurements.

A detailed study of the causes of the sudden motion identified a shock/vortex interaction as the cause. The presence and impact of this interaction was studied in terms of the Rossby number of the vortex and the axial flow properties. The lack of detailed experimental measurements was highlighted and the need for more detailed pressure surface measurements to characterize the shock wave more precisely and for velocity measurements of the vortex axial flow was argued.

One of the continuing themes that ran through the research work summarized here was a need for more detailed experimental data to aid in understanding the shock/vortex interaction being investigated. For the most part, the experimental results shown were collected before significant computational simulations were performed for the delta wing at transonic speeds, and it is fair to say that the CFD simulations played little or no roll in the planning or execution of the experiments. This is how experimental research has typically been performed historically, and in the case of the shock/vortex interaction aspects of VFE-2, we were constantly frustrated by a lack of experimental data in the region of interest. This is not the fault of the experimentalists, because the model, pressure taps, PIV locations, etc., were chosen to give a broad coverage to all the flowfields being tested, not just the transonic case in which we were interested.

A careful review of the paper, however, shows that the CFD researchers would have liked a great deal more experimental data, including flow visualization of vortex breakdown, a larger density of surface pressure measurements, shock visualization and offsurface pressure measurements across the shock, and vortex core measurements (e.g., more detail on the vortex core velocities than was available for the comparison shown in Fig. 17). Of course, we did not know that we wanted to see these specific measurements until after the CFD simulations were complete and had been analyzed. This points to a better way to conduct these studies in the future, using an integrated approach to computations and experiments, in which the are conducted in parallel, with a great deal of interaction between the computational investigators and the experimentalists. It is hoped that

Table 5 Critical incidence for transonic vortex breakdown to be found on 65 deg delta wings

Source	Type	Conditions	α_{cr}
Elsenaar and Hoeijmakers [2]	Experiment	$M = 0.85$, $Re = 9 \times 10^6$	23 deg
Houtmann and Bannink [17]	Experiment	$M = 0.85$, $Re = 3.6 \times 10^6$	20 deg
Chu and Luckring [9]	Experiment	$M = 0.799$, $Re = 6 \times 10^6$	26.6 deg
Chu and Luckring [9]	Experiment	$M = 0.831$, $Re = 6 \times 10^6$	24.6 deg
Chu and Luckring [9]	Experiment	$M = 0.851$, $Re = 6 \times 10^6$	24.6 deg
Chu and Luckring [9]	Experiment	$M = 0.871$, $Re = 6 \times 10^6$	24.7 deg
Chu and Luckring [9]	Experiment	$M = 0.9$, $Re = 6 \times 10^6$	22.6 deg
Chu and Luckring [9]	Experiment	$M = 0.849$, $Re = 11.6 \times 10^6$	24 deg
Longo [3]	CFD	$M = 0.8$, Inviscid	25 deg
Glasgow	CFD	$M = 0.85$ $Re = 6 \times 10^6$	20 deg
EADS-MAS	CFD	$M = 0.85$ $Re = 6 \times 10^6$	21 deg

future programs such as CFE-2 can take advantage of integrating computations and experiments to improve their knowledge of the flowfields being studied.

Acknowledgments

Lucy Schiavetta acknowledges the sponsorship of BAE Systems and Engineering and Physical Sciences Research Council (EPSRC), including grants EP/E009956 and GR/S16485. The third author appreciates the computational resource support provided by the U.S. Department of Defense High Performance Computing program and the Modeling and Simulation Research Center at the U.S. Air Force Academy. The authors would like to thank Dietrich Hummel for his organization of the Vortex Flow Experiment 2, which provided the framework for this study.

References

[1] Jobe, C. E., "Vortex Breakdown Location over 65 Deg Delta Wings Empiricism and Experiment," *The Aeronautical Journal*, Vol. 108, No. 1087, Sept. 2004, pp. 475–482.

[2] Elsenaar, A., and Hoeijmakers, H. W. M., "An Experimental Study of the Flow over a Sharp-Edged Delta Wing at Subsonic and Transonic Speeds," *Vortex Flow Aerodynamics*, CP-494, AGARD, Neuilly-sur-Seine, France, July 1991, pp. 15.1–15.19.

[3] Longo, J. M. A., "Compressible Inviscid Vortex Flow of a Sharp Edge Delta Wing," *AIAA Journal*, Vol. 33, No. 4, Apr. 1995, pp. 680–687. doi:10.2514/3.12631

[4] Thomer, O., Schröder, W., and Krause, E., "Normal Shock Vortex Interaction," *Symposium on Advanced Flow Management*, Pt. A, RTO-MP-069(I), NATO Research and Technology Organisation, Neuilly-sur-Seine, France, 2001, pp. 18.1–8.10.

[5] Donohoe, S. R., and Bannink, W. J., "Surface Reflective Visualisations of Shock-Wave/Vortex Interactions Above a Delta Wing," *AIAA Journal*, Vol. 35, No. 10, Oct. 1997, pp. 1568–1573. doi:10.2514/2.12

[6] Elsenaar, A., Hjemberg, L., Bütefisch, K.-A., and Bannink, W. J., "The International Vortex Flow Experiment," *Validation of Computational Fluid Dynamics*, Vol. 1, CP-437, AGARD, Neuilly-sur-Seine, France, 1988, pp. 9.1–9.23.

[7] Hummel, D., and Redeker, G., "A New Vortex Flow Experiment for Computer Code Validation," *Symposium on Advanced Flow Management*, Pt. A, RTO-MP-069(I), NATO Research and Technology Organisation, Neuilly-sur-Seine, France, 2001, pp. 8.1–8.32.

[8] Hummel, D., "Effects of Boundary Layer Formation on the Vortical Flow Above Slender Delta Wings," NATO Research and Technology Organisation, Rept. RTO-MP-AVT-111, Neuilly-sur-Seine, France, Oct. 2004, pp. 30.1–30.22.

[9] Chu, J., and Luckring, J. M., "Experimental Surface Pressure Data Obtained on a 65 Deg Delta Wing Across Reynolds Number and Mach Number Ranges," Vol. 1, NASA Langley Research Center, TM 4645, Hampton, VA, Feb. 1996.

[10] Chu, J., and Luckring, J. M., "Experimental Surface Pressure Data Obtained on a 65 Deg Delta Wing Across Reynolds Number and Mach Number Ranges," Vol. 2, NASA Langley Research Center, TM 4645, Hampton, VA, Feb. 1996.

[11] Chu, J., and Luckring, J. M., "Experimental Surface Pressure Data Obtained on a 65 Deg Delta Wing Across Reynolds Number and Mach Number Ranges," Vol. 3, NASA Langley Research Center, TM 4645, Hampton, VA, Feb. 1996.

[12] Chu, J., and Luckring, J. M., "Experimental Surface Pressure Data Obtained on a 65 Deg Delta Wing Across Reynolds Number and Mach Number Ranges," Vol. 4, NASA Langley Research Center, TM 4645, Hampton, VA, Feb. 1996.

[13] Kroll, N., Aumann, P., Bartelheimer, W., Bleecke, H., Eisfeld, B., Lieser, J., Heinrich, R., Kuntz, M., Monsen, E., Raddatz, J., Reisch, U., and Roll, B., "Flower Installation and User Handbook," DLR, German Aerospace Center, Braunschweig, Germany, 1998.

[14] Kok, J. C., and Spekreijse, S. P., "Efficient and Accurate Implementation of the k-ω Turbulence Model in the NLR Multi-Block Navier-Stokes System," *Proceedings of ECCOMAS 2000*, European Community in Computational Methods in Applied Science, 11–14 Sept. 2000.

[15] Badcock, K. J., Richards, B. E., and Woodgate, M. A., "Elements of Computational Fluid Dynamics on Block Structured Grids Using Implicit Solvers," *Progress in Aerospace Sciences*, Vol. 36, Nos. 5–6, 2000, pp. 351–392. doi:10.1016/S0376-0421(00)00005-1

[16] Leonard, A., "Energy Cascade in Large Eddy Simulation of Turbulent Fluid Flow," *Advances in Geophysics*, Vol. 18A, No. ??, 1974, pp. 237–248.

[17] Houtman, E. M., and Bannink, B. J., "Experimental and Numerical Investigation of the Vortex Flow over a Delta Wing At Transonic Speeds," *Vortex Flow Aerodynamics*, CP-494, AGARD, Neuilly-sur-Seine, France, July 1991, pp. 5.1–5.11.

[18] Schiavetta, L. A., Boelens, O. J., and Fritz, W., "Analysis of Transonic Flow on a Slender Delta Wing Using CFD," 24th AIAA Applied Aerodynamics Conference, AIAA Paper 2006-3171, June 2006.

[19] Fritz, W., and Cummings, R. M., "What Was Learned from the Numerical Simulations for the VFE-2," 46th AIAA Aerospace Sciences Meeting and Exhibit, AIAA Paper 2008-0399, Jan. 2008.

[20] Schiavetta, L., Boelens, O., Crippa, S., Cummings, R., Fritz, W., and Badcock, K., "Sting Effects on Vortex Breakdown In Transonic Delta Wing Flows," 46th AIAA Aerospace Sciences Meeting, AIAA Paper 2008-0395, Jan. 2008.

[21] Délery, J. M., "Aspects of Vortex Breakdown," *Progress in Aerospace Sciences*, Vol. 30, No. 1, 1994, pp. 1–59. doi:10.1016/0376-0421(94)90002-7

[22] Kalkhoran, I. M., and Smart, M. K., "Aspects of Shock Wave-Induced Vortex Breakdown," *Progress in Aerospace Sciences*, Vol. 36, No. 1, 2000, pp. 63–95. doi:10.1016/S0376-0421(99)00011-1

[23] Spall, R. E., Gatski, T. B., and Grosch, C. E., "A Criterion for Vortex Breakdown," *Physics of Fluids*, Vol. 30, No. 11, Nov. 1987, pp. 3434–3440. doi:10.1063/1.866475

[24] Robinson B. A, Barnett R. M, and Agrawal, S., "Simple Numerical Criterion for Vortex Breakdown," *AIAA Journal*, Vol. 32, No. 1, Jan. 1994, pp. 116–122. doi:10.2514/3.11958